Central impurity convection and its connection to MHD activity in ASDEX Upgrade

M. Sertoli, V. Igochine, A. Gude, R. McDermott and ASDEX Upgrade Team

Max-Planck-Institut für Plasmaphysik, EURATOM Association, Garching, Germany

Introduction

Central electron cyclotron resonance heating (ECH) is routinely used in H-mode discharges at ASDEX Upgrade (AUG) to avoid tungsten accumulation in the plasma centre, but the underlying physics mechanisms responsible for this are still not clear. The turbulent theories which predict the rise of an outward impurity convection in the plasma centre in the presence ECH [1] require a nested flux surface geometry and are not applicable inside the $q = 1$ surface where strong MHD activity is usually present. Moreover, a relationship between central ECH and mitigation of impurity accumulation with a change in characteristics of the $(m,n) = (1,1)$ sawtooth precursor has been previously reported [2, 3]. Mode-ion interaction could lead to an expulsion of impurities from inside the $q = 1$ surface (e.g. through polarization drift). Such processes depend strongly on the mode frequency in the plasma frame $\omega = \omega_{mode} - \omega_{rot}$ (where ω_{mode} and ω_{rot} are the mode and plasma toroidal rotation frequencies in the laboratory frame) so precise toroidal rotation measurements from charge exchange recombination spectroscopy (CXRS) are required. Recent discharges have shown discrepancies of up to 20% in ω_{rot} evaluated by the CHR system with respect to the recently upgraded CER diagnostic. Since only CHR was available for the considered cases, such a discrepancy would lead to a 100% error in the evaluation of ω. For this reason, analysis of mode-tungsten interaction is not reported. A characterization of typical sawtooth (ST) cycles in the absence/presence of central ECH is given and a proof of principle of a simple method to evaluate intrinsic tungsten density inside the plasma core through the combined use of CXRS and soft X-ray diode (SXR) measurements is explained.

Experimental Results

Three typical ST cycles are analysed from two discharges with $I_p = 1$ MA, $B_t = 2.5$ T, $q_{95} = 4.6$ and central line averaged density $\overline{n}_e \sim 8 \cdot 10^{19}\ m^{-3}$. Figure 1 shows the spectrograms of the most

Discharge	P_{NBI} (MW)	P_{ECH} (MW)	ρ_{ECH}	$\rho_{q=1}$	τ_{ST} (ms)	c_W	c_C	c_{Ar}
25447 (a)	5	-	-	0.23	100	$2{\cdot}10^{-5}$	$5{\cdot}10^{-3}$	$6{\cdot}10^{-6}$
24681 (b)	5	0.7	0.16	0.30	40	$2.5{\cdot}10^{-5}$	$1{\cdot}10^{-2}$	-
24681 (c)	10	0.7	0.24	0.27	130	$2{\cdot}10^{-5}$	$1{\cdot}10^{-2}$	-

Table 1: *Discharge number; NBI and ECH power; position of ECH deposition and of the q=1 surface in normalized poloidal flux radial coordinates (ρ_{ECH} and $\rho_{q=1}$ respectively); average sawtooth period (τ_{ST}); measured tungsten, carbon and argon impurity concentrations of the analysed discharges.*

central line of sight (LOS) of the SXR camera H (H53) for the three cases, which from now on will be referred to as "peaked" (a), "flat" (b) and "hollow" (c).

The peaked (reference) case is the classical ST cycle with a long quiescent phase and an exponential growth of the mode shortly before the crash. Such cycles appear mainly when no central ECH is present. Both the SXR emissivity and electron temperature profiles peak (with respect to the profile just after the crash, ΔP_{SXR} and ΔT_e in figure 2a) throughout the whole cycle until the crash occurs. By tracking the mode frequency in the spectrogram of each ECE channel, the time evolution of the radial mode structure can be analysed ($\delta T_e/T_e$ in figure 2a). The $q = 1$ radius (dashed vertical line) has been estimated from the mode amplitude and phase profiles. Since the electron density profile in the centre varies less than a few percent, the peaking of the

SXR emissivity profile is to be attributed to a peaking in impurity density. A proof of this will be given in the next section.
Case (b) shows instead a flat SXR emissivity profile throughout the full cycle while T_e peaks at approximately the same value as in the reference case ($\sim$ 15%). The mode appears early and saturates at $\sim$ 2.245 s, the crash occurring $\sim$ 30 ms later. All the channels of the ECE diagnostic have the same phase (cosine of the channel phase in reference to the phase of the most central channel $cos(\phi_{ECE} - \phi_{ECE}(r_{min}))$ in figure 2b) suggesting the mode is ideal. This is confirmed by the peaking of T_e since the ECH deposition radius ($\rho_{ECH} \sim 0.16$) is well inside the $q = 1$ surface. The density profile behaves as in the reference case.
In the hollow case an early rise of the (1,1) mode is also visible, but both the SXR and the ECE profiles show a very different time evolution. While T_e remains approximately flat inside $q = 1$, the SXR profile peaks slightly until the mode saturation ($\sim$ 4.58 s, visible in the $\delta T_e/T_e$ plot in figure 2) when a strong decrease in central SXR emissivity occurs leading to an "accumulation" at (or slightly outside) the $q = 1$ surface which lasts up to the crash. A phase jump of $\sim \pi$ (right plot in figure 2c) observed around $\rho_{q=1}$ suggest that this (1,1) mode is of resistive nature. This is also in line with a flat T_e profile inside $q = 1$ since the presence of an island would lead to an increased heat transport through the island x-point. The n_e profile behaves as in the previous cases but exhibits a strong flattening at the end of the cycle suggesting that all ion species may be somewhat affected in the expulsion process. Alternating hollow and flat cycles with constant heating have also been observed. The process governing the flattening and hollow nature of the impurity density profiles could therefore be the same but only if the mode is resistive would the impurity find direct access to the radii outside of the $q = 1$ surface through the x-point of the island.

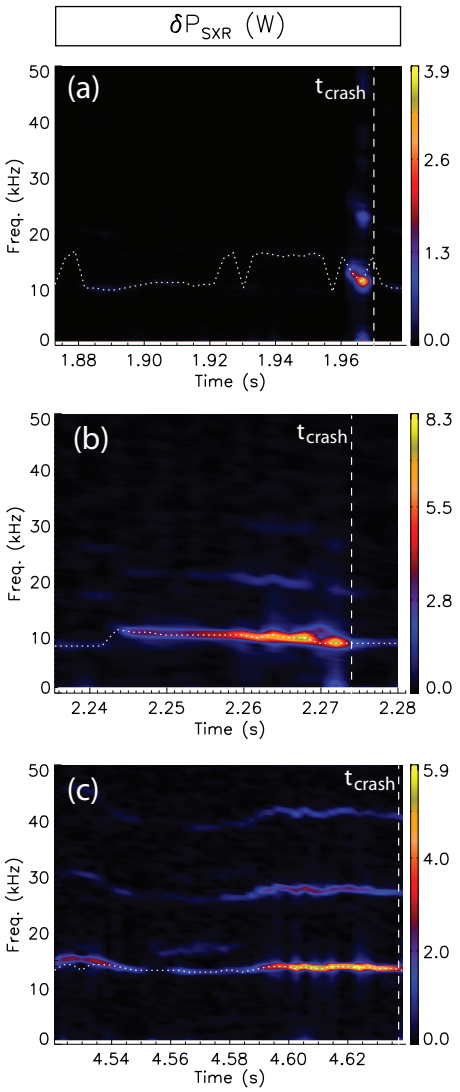

Figure 1: *Spectrogram of SXR central LOS H53 for the three cases (labels as in table 1). Horizontal dashed white line indicates mode frequency tracking, vertical one the ST crash time.*

Since the spectroscopically evaluated average central tungsten concentration is $\sim 2 \cdot 10^{-5}$, the mode stability may not be expected to be modified by a change in impurity density profiles. From the point of view of linear stability, such tungsten concentrations will affect neither the pressure nor the current terms in the MHD potential energy. Effects due to a degradation of the temperature profiles via strong impurity radiation may also be expected to be negligible in such low concentration regimes.

Evaluation of the tungsten density

The light detected by the SXR diode diagnostic can be modelled as:

$$\varepsilon_{SXR}(r,t) = n_e(r,t) \sum_Z n_Z(r,t) L_Z^{SXR}(T_e(r,t), n_e(r,t)) \quad (1)$$

where n_e is the electron density, n_Z is the density of the ion species with atomic number Z, L_Z^{SXR} represents the total radiated power (also called cooling factor) of the element per unit electron and ion densities ($photons \cdot m^3 \cdot s^{-1}$) filtered according to the filter function of the

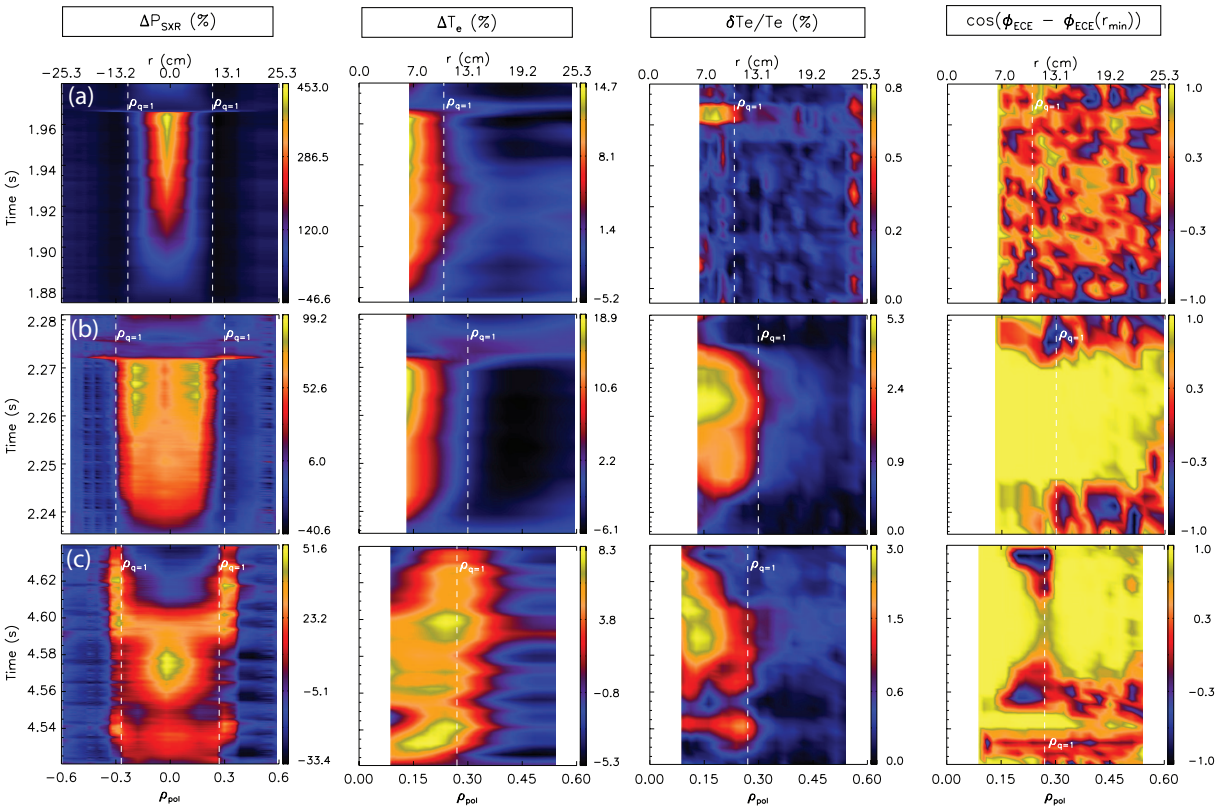

Figure 2: *Time evolution of the change in SXR emissivity during the ST cycle [ΔP_{SXR}] and in ECE electron temperature profiles [ΔT_e] with respect to the start of the cycle; normalized mode amplitude from ECE [$\delta T_e/T_e$]; mode phase from ECE with respect to the central channel [$cos(\phi_{ECE} - \phi_{ECE}(r_{min}))$].*

diagnostic. All information on n_e and T_e is contained in these emissivity coefficients. Since the sum is performed over all ion species emitting in this spectral range (including deuterium), an exact evaluation of eq. 1 would require the knowledge of the main ion density as well as that of all the impurities. Since the main impurity species present in the plasma are *He*, *C*, *O*, *B* and *W*, in first approximation the sum can be restricted to these. If the densities of the light impurities are known, the deuterium density can be evaluated through the quasi-neutrality condition $n_D = n_e - \sum_Z n_Z \cdot Z$. Only the low-Z impurities will participate since the concentration of heavy ones is very low. These impurities will be completely ionized in the plasma centre, so the sum can be done over the atomic number.

After having performed a deconvolution of the experimental SXR emissivity to evaluate the local profile $\varepsilon_{SXR}(r,t)$, the only unknown in equation 1 will be the tungsten density:

$$n_W = (\frac{\varepsilon_{SXR}}{n_e} - n_D L_D^{SXR} - n_{He} L_{He}^{SXR} - n_C L_C^{SXR} - n_O L_O^{SXR} - n_B L_B^{SXR})/L_W^{SXR} \quad (2)$$

Since time resolved low-Z impurity ion densities can be experimentally evaluated with CXRS data, this equation can be solved for successive time-points and the time evolution of the intrinsic n_W profile recovered, enabling the determination of the time evolution of the intrinsic tungsten density at the CXRS time resolution. If more than one CXRS system is present, the densities of more than one impurity can be determined experimentally and the solution requires less assumptions.

For the cases analysed, only carbon was measured using the CHR system. Oxygen $c_O = c_C/10$ and helium $c_{He} = 1\%$ concentrations were assumed for all cases. Case (a) was performed 10 days after a boronization so $c_B = c_C$ was assumed. Argon was also present in this case and

detected by a Johann spectrometer ($c_{Ar} = 6 \cdot 10^{-6}$). The shapes of these density profiles are assumed equal to that of carbon. Because of a 50 ms time resolution of the CXRS system, no time resolved evaluation was performed. To test the method, a time average of all quantities has been performed over three consecutive ST cycles. Error bars in n_e and T_e have been neglected to study the propagation of CXRS errors on the evaluation of the n_W. In first approximation, the SXR diode data has been Abel-inverted neglecting possible HFS-LFS asymmetries due to centrifugal forces acting on the tungsten ions and has been then divided by a normalization factor of 12 previously evaluated through a comparison with spectroscopic data [4]. The results are shown in the left plots in figure 3. Despite the large error bars in the CXRS data, the tungsten density is clearly peaked in the first case, while hollow in the second two, with the peak moving towards the $q = 1$ surface for case (c). Despite such low tungsten densities, its contribution to the SXR emissivity reaches peaks of 60%. The other main players are deuterium (dark blue), carbon (red) and boron (light blue) close after boronization, all other impurities contributing less than 10%. A comparison of the evaluated n_W with the values measured by the grazing incidence spectrometer has been done by averaging the n_W density for radii smaller than the detection limit of the diagnostic (approximately at $\rho \sim 0.5$). This leads to concentrations of $2.2 \cdot 10^{-5}$, $2.4 \cdot 10^{-5}$ and $2 \cdot 10^{-5}$ for cases (a), (b) and (c), respectively, which can be compared to the measured values of $2 \cdot 10^{-5}$, $2.6 \cdot 10^{-5}$ and $3 \cdot 10^{-5}$. These values are extremely close considering the assumptions made and to some extent validate the assumption that the SXR emissivity profile shape follows closely that of the impurity density.

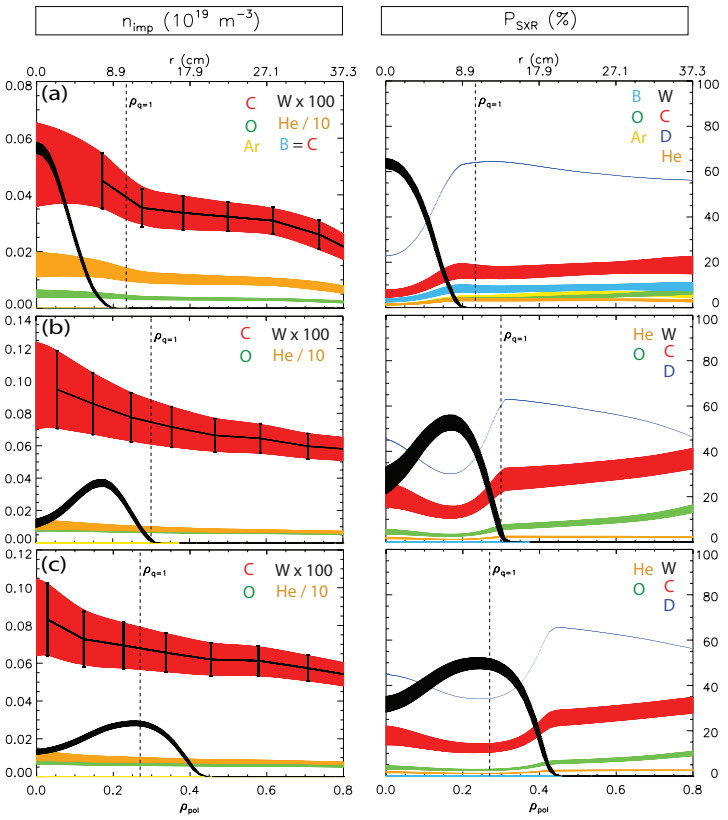

Figure 3: *Left: impurity densities, the CXRS carbon densities in red with black error bars. n_W is multiplied by 100, n_{He} devided by 10 for visualization purposes. Right plots: fraction of the SXR emissivity due to each ion.*

Outlook

Through the simple method outlined above and the recently upgraded CXRS-system CER, the time evolution of intrinsic tungsten density will be calculated for different ECH heating schemes and NBI-only cases. This will clarify if the time evolution of the low-Z impurities is the same as that of tungsten or if the flattening/expulsion effect seen for ST cases (b) and (c) is a special feature of tungsten only. This will also provide information important to understand what physical processes govern the flattening and expulsion during mode saturation.

References

[1] C. Angioni and A. G. Peeters, Physical Review Letters **96**(9), 095003–1 (2006).
[2] J. Stober et al., EPS 2007 , P–5.138 (2007).
[3] A. Gude et al., EPS 2010 , P–4.124 (2010).
[4] M. Sertoli et al., Plasma Physics and Controlled Fusion **53**(3), 035024 (2011).